Dynamic Mechanical and Raman Spectroscopy Studies on Interaction between Single-Walled Carbon Nanotubes and Natural Rubber

M. A. López-Manchado,[1] J. Biagiotti,[2] L. Valentini,[2] J. M. Kenny[2]

[1]*Institute of Polymer Science and Technology, C.S.I.C. C/Juan de la Cierva, 3 28006, Madrid, Spain*
[2]*Materials Science and Technology Center, INSTM Unit, Università di Perugia, Loc. Pentima bassa, 21-05100 Terni, Italy*

Received 17 January 2003; accepted 5 September 2003

ABSTRACT: The effects of the incorporation of single-walled carbon nanotubes (SWNTs) on the physical and mechanical properties of natural rubber (NR) are described. Characterization of these new materials has been performed by dynamic mechanical analysis, differential scanning calorimetry, and Raman spectroscopy to obtain information about of the possible interactions between both materials as well as the dispersion of SWNTs on elastomer matrix. The results are then compared with those obtained for NR–carbon black composites. Dynamic mechanical analysis indicates a stronger filler–matrix interaction in the case of SWNTs incorporation, showing a noticeable decrease of the height of tan δ peak, as well as a marked shift of T_g towards higher temperatures. In particular, the increase of the storage modulus indicates a beneficial effect of SWNTs incorporation with respect to NR filled with carbon black and the pristine polymer matrix. In addition, calorimetric analysis indicates that both fillers accelerate the NR vulcanization reaction, this effect being more evident when SWNTs are added into the matrix. Raman spectroscopy indicates that SWNTs dispersion into the elastomer matrix creates residual strain on the nanotubes bundle. We demonstrate that the Raman microprobe technique provides a means for load transfer effectiveness of SWNTs. © 2004 Wiley Periodicals, Inc. J Appl Polym Sci 92: 3394–3400, 2004

Key words: Raman spectroscopy; mechanical properties; carbon nanotubes; nanocomposite

INTRODUCTION

The concept of reinforcement for rubbers is complex to define, but may be considered as the enhancement of the modulus, failure properties (tensile and tear strength), and abrasion resistance of the vulcanizates. Hence, the main goal for filler addition is to improve certain properties and cheapen the compound. Among several fillers, carbon black (CB) is the most important reinforcing agent used in the rubber industry. Because of its own organic nature, carbon black is compatible with the elastomer matrix. On the other hand, it is well known that the particle size, structure, and surface characteristics of the fillers are the main factors controlling their reinforcing ability, in particular, the particle size. In this sense single-wall nanotubes (SWNTs) are believed to be the ultimate reinforcement material in polymer composites, due to their high aspect ratio (up to 10^4), Young's modulus ($\sim 10^3$ GPa) close to that of diamond,[1] tensile strength of ~50 GPa,[2] and light weight (density of ~1.3 g/cm^3).[1–5]

In practice, preparation of high-strength nanocomposites has yet to overcome several obstacles. SWNTs form different diameter crystalline nanoropes that usually exhibit bends and loops. As the rope diameter increases, shear deformation reduces the effective moduli of nanoropes by an order of magnitude with respect to that of a SWNT. Therefore, controllable dispersion and alignment of SWNTs in composites are desirable to achieve improvement of the mechanical properties. In addition, interface region properties are known to be crucial for load sharing between the matrix and the reinforcement material. There is little knowledge of the interface region in nanocomposites, because direct studies[2,4] are obstructed by the nanosize diameter and high aspect ratio of a SWNT/rope.

The main goal of this work is to make a comparison between the physical and mechanical properties of SWNTs and CB-filled natural rubber composites. The thermal characterization was performed by means of differential scanning calorimetry (DSC). The mechanical behavior of the composites was studied using a dynamic mechanical analyzer. The application of Raman spectroscopy for nondestructive studies of residual strains and load transfer in nanocomposites was reported.

Correspondence to: J. M. Kenny (kenny@unipg.it).
Contract grant sponsor: the Ministerio de Ciencia y Tecnología in the form of the Ramón y Cajal grant (to M.A.L.-M.).

© 2004 Wiley Periodicals, Inc.

TABLE I
Formulations of the Rubber Compounds

Natural rubber	100	100	100
Zinc oxide	5	5	5
Stearic acid	1	1	1
Sulfur	2.5	2.5	2.5
MBTS[a]	1	1	1
PBN[b]	1	1	1
Carbon black	—	10	—
SWNTs	—	—	10

[a] Benzothiazyl disulfide
[b] Phenyl beta naphtyl amine

EXPERIMENTAL DETAILS

Natural rubber was generously supplied by Malaysian Rubber under the trade name CV 60 (Mooney viscosity, ML (1+4) 100°C 60). SWNTs were commercially obtained from CarboLex. The material consisted of packed bundles of SWNTs of 12–20 Å in diameter. There were approximately 30 nanotubes per bundle (with an average bundle diameter of 100 Å), with a length of several micrometers. Carbon black was generously supplied by Cabot, S.A. under the trade name Spheron 6400 (DBP 100 cc/100 g).

Rubber compounds were prepared in an open two-roll mill at room temperature. The rotors operated at a speed ratio of 1:1,4. The vulcanization ingredients were added to the elastomer previously to the incorporation of the filler, and finally, the sulphur was incorporated. The amount of carbon black and SWNTs were 10 part per hundred (phr) of rubber. The formulation of the compounds are described in Table I.

Dynamic mechanical properties of the solid polymer (25 × 4 × 0.5 mm) were determined using a dynamic mechanical thermoanalyzer Metravib model Mark 03. Tests were carried out in torsion deformation mode, at a frequency of 5 Hz, and the temperature programs were run from −80 to 30°C, at a heating rate of 2°C/min, under a controlled sinusoidal strain in a flow of nitrogen. At least three samples for each concentration were prepared and tested.

DSC measurements were carried out on a Mettler Toledo differential scanning calorimeter model DSC 822. The curing reaction was evaluated under isothermal and dynamical conditions. Isothermal curing was performed at five different temperatures: 160, 170, 180, 190, and 200°C, and dynamic testing was evaluated at six heating rates: 2, 5, 10, 15, 25, and 50°C/min. The weight of the samples was in the range of 15–20 mg. To confirm the thermal properties of the composites at least three samples for each filler concentration were prepared and tested.

Raman scattering spectra were recorded by a Jobin Yvon micro-Raman LabRam system in a backscattering geometry on vulcanized samples. A 632.8 nm (1.96 eV) He-Ne laser was used as the light source, and the power of the laser was adjusted by optical filters. By using a 100× objective lens, the illuminated spot on the sample surface was focused to about 2-μm diameter. The resolution of Raman spectra was better than 1 cm^{-1}.

RESULTS AND DISCUSSION

Dynamic mechanical properties of neat NR and its composites with carbon black and SWNTs were studied over a wide temperature range (−80 to 30°C). The variation of the tan δ as a function of the temperature, for all studied materials is reported in Figure 1. By incorporating of fillers, the height of tan δ peak, corresponding to the glass transition temperature (T_g) of the elastomer, is reduced. In fact, at low temperatures the fillers give a lower hysteresis for a given energy input. This is particularly evident in the case of SWNTs. However, at high temperatures (room temperature), no significant changes are observed. This behavior was explained by Wang[6] in terms of a reduction in polymer fraction in the composite. That is, at low temperatures, the polymer itself is the responsibility of the high portion of energy dissipation, while the small solid filler particles in the polymer matrix hardly absorb energy. This explanation is reasonable for hysteresis in the transition zone, but it is not true at high temperatures (rubbery state), where the hysteresis tend to increase in the presence of the fillers. This is due to the fact that the filler network can be broke down, causing an additional energy dissipation, and consequently, a higher hysteresis in the rubbery region. In addition, a shift of the tan δ peak towards higher temperatures by addition of the fillers is observed. So, T_g goes from −49.4 for pristine NR to −46.7 for the NR-CB composite and −45.7 for NR-SWNTs composite. These results are in good agreement with those reported elsewhere.[7,8] This indicates a strong interfacial action between the filler and matrix,[9–11] in particular, by incorporation of SWNTs. This

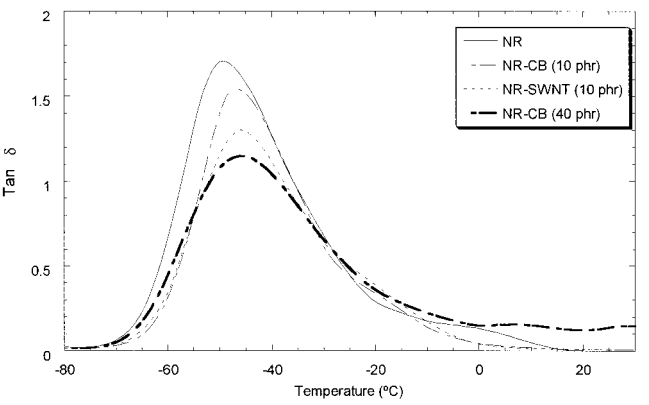

Figure 1 Tan δ traces as a function of the temperature for all studied materials.

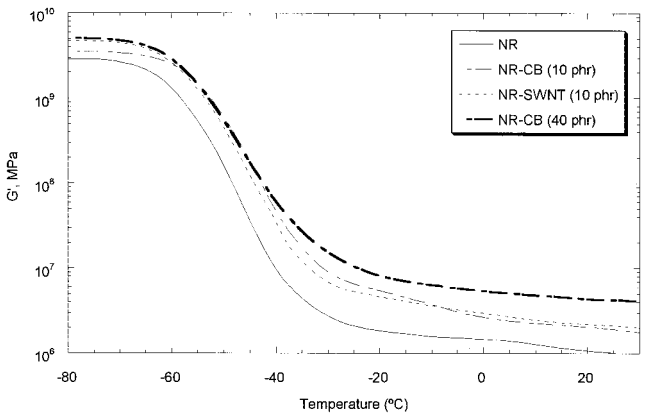

Figure 2 Variation of the storage modulus as a function of the temperature for all studied materials.

interaction restricts the mobility of the elastomer segments, which significantly elevated glass transition temperature. This rubber portion immobilized (occluded rubber) acts as a part of the filler rather than of the polymer, and increases the effective volume of the filler.

Figure 2 shows the storage modulus (the elastic component of the complex modulus) as a function of the temperature for NR and its compounds at 10 phr filler loading. It can be easily seen that the modulus sensibly increases in the presence of both fillers, which is attributed to the hydrodynamic reinforcement upon introducing the filler. It is well known that the hydrodynamic reinforcement occurs in the conventional fillers, giving rise to an increase in the modulus in polymer matrix or increase in the viscosity in liquids.[12] It is noteworthy that at the same filler content the reinforcing effect of the SWNTs is sensibly higher than carbon black. To highlight the beneficial effect of SWNTs incorporation, in terms of mechanical stiffness improvement, a comparison between the storage modulus of a 40 phr carbon black-filled compound and a 10-phr SWNTs–NR nanocomposite is shown in Figure 2.

The different properties between carbon black and SWNTs-filled natural rubber composites can find an explanation in terms of the dissimilar filler morphology, namely, particle size or surface area and structure. SWNTs are characterized for a higher aspect/ratio with respect to carbon black, as smaller particle size, larger interfacial area, and a stronger polymer–filler interaction can be expected in a thicker rubber shell. This leads a more immobilized rubber shell compared with large-particle carbon black. This occluded rubber acts as a filler part, and hence, increases the effective volume of filler loading, which will give rise to higher hysteresis at higher temperatures and lower hysteresis at lower temperatures. In addition, a higher filler–polymer interfacial action will increase the total bound rubber, which in combination to the higher effective volume of the aggregates could reduce the flocculation rate of small particles. Another interesting aspect to be considered for understanding the differences between both fillers is the anisometry of filler aggregates. It is assumed that the hydrodynamic reinforcement depends of the volume fraction and the shape factor of the filler particles.[9,13–15] Guth-Gold[15,16] introduced a shape factor for fillers to account for the effect of the anisometry of colloidal particles. The shape factor is described as the ratio of the longest dimension of the particle to the shortest. So, the shape factor will be larger for SWNT than its counterparts of carbon black. It is understood that in compounds containing fillers with identical surface area and chemical nature but different shape, the modulus increases with increasing anisometry. This allows explaintion of the higher modulus in the case of the compounds loaded with SWNTs compared to those with carbon black.

The effect of fillers, carbon black, and SWNTs on the NR vulcanization reaction has also been analyzed by differential scanning calorimetry (DSC) under dynamic and isothermal conditions. DSC is a major achievement in the field of analytical tools for determining the energy required during the rubber vulcanization. The analysis through DSC is based on the assumption that the heat of reaction is only due to a single curing reaction, and is proportional to the extent of the reaction. Therefore, the degree of curing can be calculated from the heat flow peak of a DSC curve.[17] Usually, the degree of cure (α), can be easily defined by the following equations:

$$\alpha = \Delta H_t / \Delta H_\infty \quad (1)$$

where α is the degree of cure, ΔH_t is the accumulated heat evolved to time t, and ΔH_∞ is the total amount of heat generated during the entire reaction.

It is well assumed that the equation describing the thermal behavior of an elastomer during a vulcanization process is obtained by appraising at each instant a thermal balance where diffusion of heat and source terms originated from the exothermic reaction occurring during the vulcanization phenomenon are taken into account. A typical cure curve is shown in Figure 3. Three regions are clearly observed. The first region is the scorch delay or induction period, during which the most of the accelerator reactions occur. The second period is due to the curing reaction, during which the network structure is formed. In the last period, the network matures by overcuring reversion, equilibrium, or additional but slower crosslinking, depending on the nature of the compound. In our case, natural rubber tends to give reactions of overcuring reversion, due to the degradation of polysulfides bonds.

Figure 4 shows the dynamic DSC curves for neat NR, where the heat flow absorbed during the vulcanization process is represented as a function of tem-

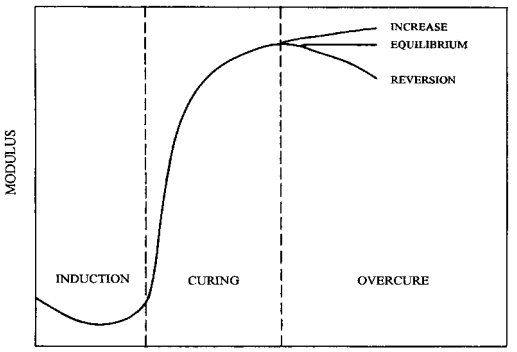

Figure 3 Typical cure curve of an elastomer.

perature, at different heating rates. As can be seen, the curing temperature increases as the heating rate increases. The temperatures of the cure peaks (T_p) for all studied materials, at the different heating rates used, are summarized in Table II. By incorporation of fillers a shift of the peak towards lower temperatures is observed. This indicates the vulcanizing ability of both fillers, this effect being more evident in the case of SWNTs.

The activation energy of the curing process was easily estimated by means of both Ozawa and Kissinger equations, which are given by the following expressions:

$$E_a = -2.3\mathrm{R}\frac{d\log q}{d(1/T_P)} \quad \text{Ozawa equation} \quad (2)$$

$$E_a = -2.3\mathrm{R}\frac{d\log(q/T_P^2)}{d(1/T_P)} \quad \text{Kissinger equation} \quad (3)$$

where T_p is the temperature of the exothermic peak and q is the heating rate. The graphic representation of the temperature peak and its derivative vs heating rate (Ozawa and Kissinger equations, respectively) gives

TABLE II
Temperatures of the Cure Peaks and E_a in Dynamic DSC Tests

Material	Heating rate (°C/min)	Temperature at peak T_p (°C)	E_a (Kcal/mol) Ozawa	Kissinger
NR	2	166.13		
	5	182.68		
	10	192.12		
	15	201.30		
	25	207.40		
	50	224.11		
			24.6	22.7
NR-carbon black	2	147.80		
	5	163.39		
	10	177.60		
	15	185.40		
	25	196.22		
	50	218.72		
			18.9	17.1
NR-SWNTs	2	143.85		
	5	157.15		
	10	173.54		
	15	181.25		
	25	193.56		
	50	214.00		
			18.2	16.4

rise to straight lines of whose slopes the activation energy of the process can be calculated (Figs. 5 and 6). The obtained results by both expressions are reported in Table II. It can be observed that the activation energy noticeably decrease in the presence of fillers. However, it is of interest to note that the SWNTs are the most effective ones. Thus, it can be concluded that SWNTs favor the processing conditions for NR, because a lower energetic requirement for vulcanizing is needed.

The kinetic of the vulcanization reactions was also evaluated, under isothermal conditions, at several temperatures. Figure 7 shows the curing curves of

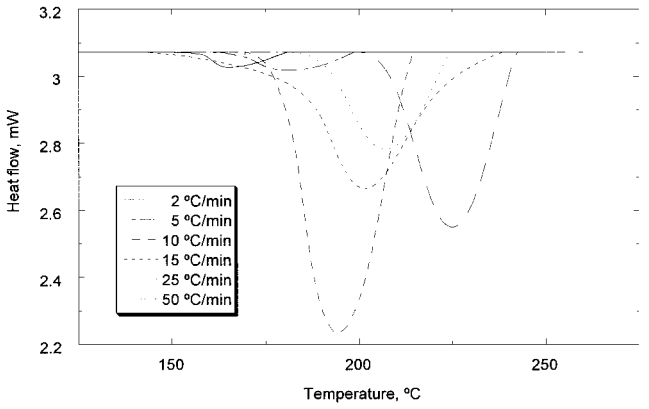

Figure 4 Dynamic DSC curves for pristine NR at different heating rates.

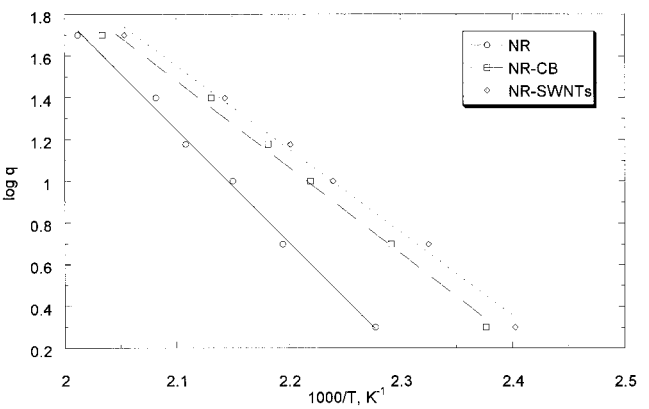

Figure 5 Calculate of E_a of vulcanization process by using Ozawa equation.

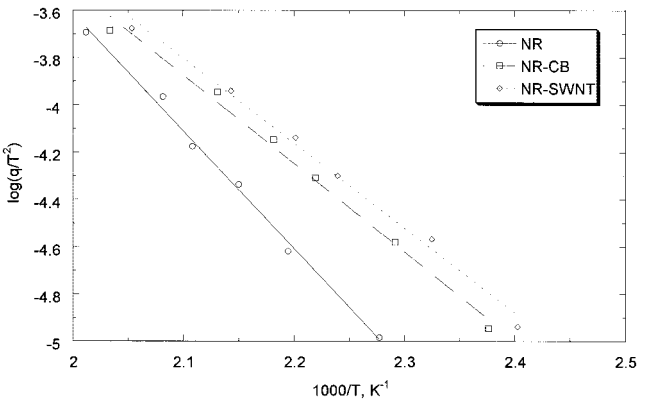

Figure 6 Calculate of E_a of vulcanization process by using Kissinger equation.

pure NR as a function of time, at different temperatures. The scorch time, t_{50} and t_{97} for all studied materials are listed in Table III. With increasing temperature, the vulcanization rate increases. To know the effect of both fillers on NR vulcanization under isothermal conditions, the curing degree curves vs time, obtained by integrating the area under the exothermic peaks, at 160°C, are graphically represented in Figure 8. It can be observed that the vulcanization reaction is accelerated in the presence of fillers. This behavior is more evident in the case of SWNTs. These results support a further strong indication of vulcanizing effect of SWNTs on NR kinetic cure, accelerating the crosslinking reaction.

Raman characterization has also been applied to highlight the effects of SWNTs on the natural rubber composites. The high frequency parts of the Raman spectra of SWNTs/NR composites are shown in Figure 9. The spectra exhibit peaks at 1275, 1549, and 1589 cm^{-1}. SWNTs G modes (1549 and 1589 cm^{-1}) shown in Figure 9(b) involve tangential C—C bond stretching motions.[18] Generically, they stem from the E_{2g2} mode

TABLE III
Cure Characteristics in Isothermal DSC Tests

Material	T_c (°C)	t_{50} (min)	t_{97} (min)
NR	160	8.90	21.20
	170	4.10	15.40
	180	2.40	10.0
	190	1.40	9.60
	200	0.72	3.48
NR-Carbon black	160	4.10	11.05
	170	3.26	9.30
	180	2.70	8.00
	190	1.35	5.20
	200	0.60	2.50
NR-SWNTs	160	3.50	8.30
	170	2.17	7.20
	180	1.60	5.40
	190	1.10	4.60
	200	0.50	2.25

at 1580 cm^{-1} in graphite: $E_{2g_2} \rightarrow A_{1(g)} + E_{1(g)} + E_{2(g)}$. The graphite-like G modes exhibit a definite upward shift after the nanotubes were embedded in the epoxy matrix. The band localized around 1275 cm^{-1} is generally assigned to the D-line of graphite, and corresponds to the disordered graphite structures.[1,18,19] The D band is activated in the first-order scattering process of sp^2 carbons by the presence of in plane substitutional hetero-atoms, vacancies, grain boundary, or other defects, and by finite size effects, all of which lower the crystalline symmetry of the quasi-infinite lattice.[20]

The Raman spectra recorded on the same samples in the low-frequency part [Fig. 9(a)] show a well-pronounced peak at around 100–200 cm^{-1}. This band is attributed to the breathing type vibration (RB modes, A_{1g} symmetry) of nanotubes, and its frequency depends on the inverse diameter. These spectra were then analyzed quantitatively by searching the minimum number of frequencies that fitted the different Raman bands without fixing the position and the

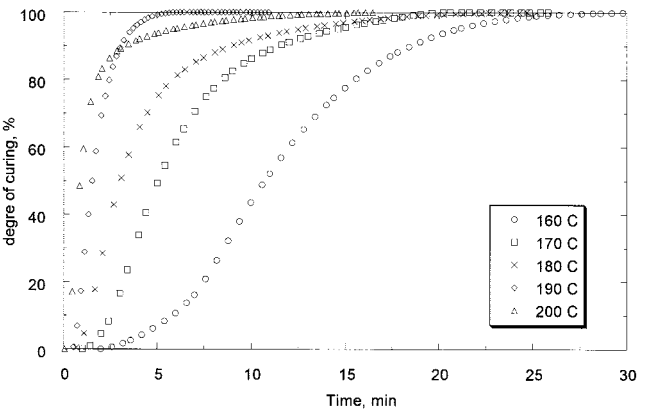

Figure 7 Degree of curing for pristine NR as a function of time, at different temperatures.

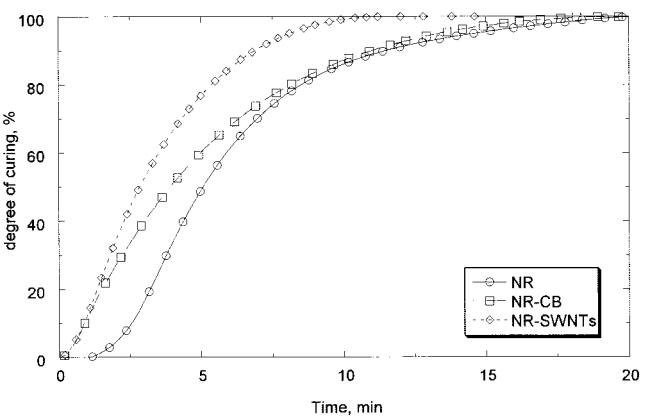

Figure 8 Degree of curing for all studied materials.

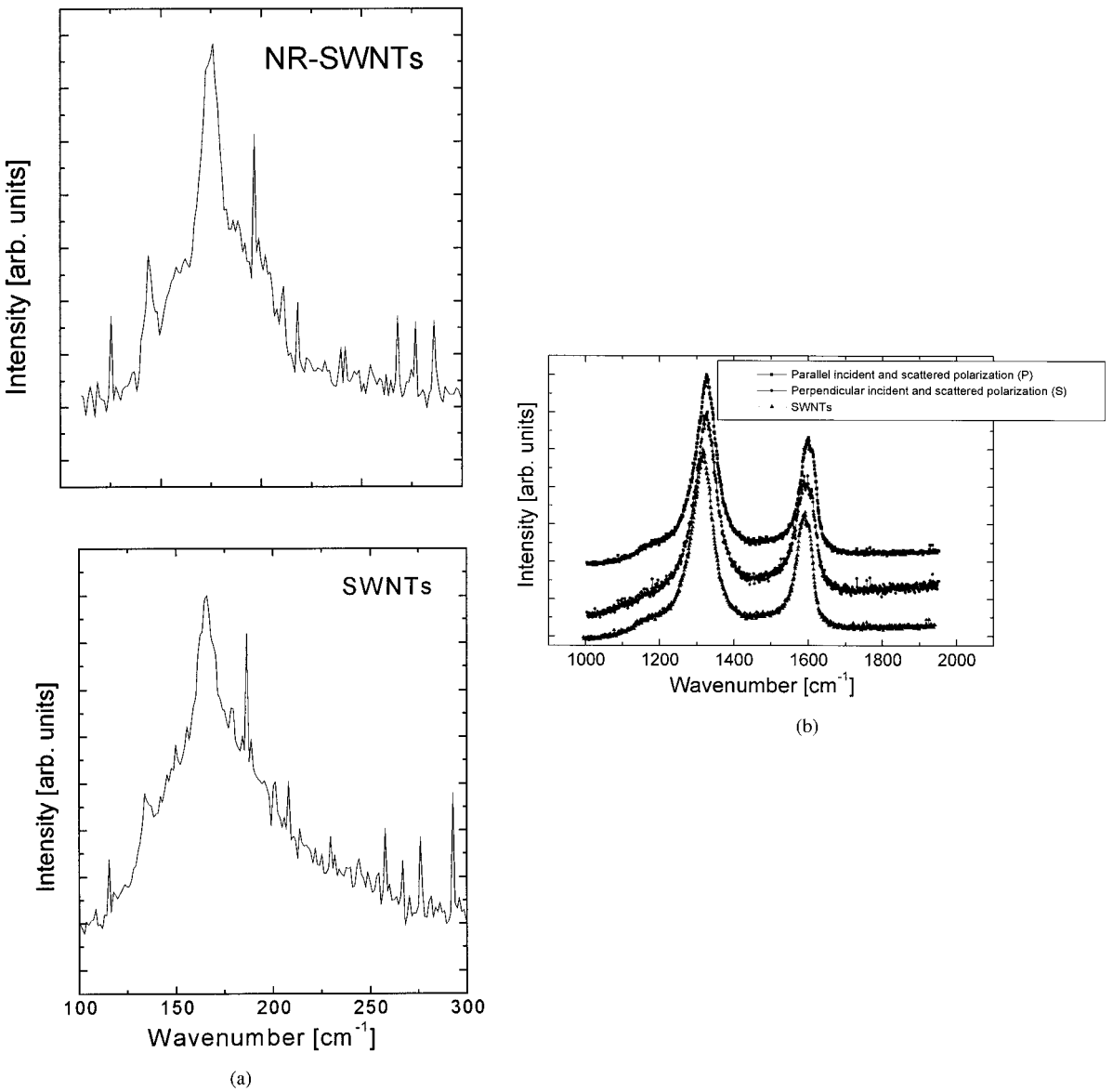

Figure 9 (a) Low-frequency Raman spectra of SWNTs and NR/SWNT composites; (b) high-frequency Raman spectra of SWNTs and NR/SWNTs composites.

widths of the individual peaks.[21–23] From Figure 9(a) it is clear that the mentioned peaks do not change in position in going from pure SWNTs to composites.

The graphite-like G modes in Figure 9(b) exhibit a definite upward shift after the nanotubes were embedded in the NR matrix. Interestingly, the G1 band position is different when measured in parallel (P) or perpendicular (S) incident and scattered light polarizations. The G1 frequency measured for the S polarization almost coincides with that of pure SWNTs and does not depend on the compressive strain applied in the vulcanization process. In fact, the polymer exerts a pressure on the individual tubes increasing the tangential mode frequencies. In contrast, the P-polarized G1-peak position shifts upward by 10 cm^{-1}. We note that the Raman intensity measured in parallel polarizations is dominated by scattering from SWNTs aligned along the incident polarization direction. A similar effect was found by Hadjiev et al.,[24] which shows how a shift of 3 cm^{-1} of the P-polarized G1-peak position demonstrates the load transfer effectiveness of SWNTs ropes embedded in a nanocomposite. It is interesting to note that in the case of NR/CB composite G1 band position (located at about ≈1592 cm^{-1}) does not exhibit significant change for the S and P polarization.

We summarize the experimental findings as follows: (1) the RB-band frequency does not change in going from purified SWNTs to composites; (2) the G1 modes exhibit an upward shift after NR vulcanization; (3) tensile stress exerted by polymer intercalation induces strain on SWNTs that are oriented along the

applied stress direction, whereas the strain on the perpendicularly aligned nanotubes remains unchanged within experimental resolution; and (4) composite loads the CB to the strain it have in the unstressed specimen.

From the aforementioned findings, we conclude that the observed shift of the G modes and absence of frequency change for the RB modes excludes from consideration a Van der Waals type mechanism that is found to govern the RB-and G-modes shift under hydrostatic pressure. Rather, it suggests a direct coupling of SWNTs/ropes to the NR matrix.

We note that although the findings (3) may hint at the decoupling of the SWNTs as a result of the tensile stress, those in (4) evidence more for a deformation of the matrix after the vulcanization that, however, preserves CB–matrix coupling.

CONCLUSIONS

The physical and mechanical properties of single-walled carbon nanotube reinforced natural rubber were analyzed in the present work. It was shown how the incorporation of SWNTs accelerates the NR vulcanization reaction, and how this change is very important to interpret the function of the nanotubes as reinforcement in composite materials.

Dynamic-mechanical analysis confirmed the reinforcing effects of the nanotubes on elastomer matrix. In fact, the incorporation of low concentrations of SWNTs gives rise to a more rigid material, which is reflected in a marked increase of the storage modulus. This effect is not noticeable with equal carbon black dispersion in the blend. A tangential active Raman mode supports the important findings reported here: the load is transferred predominantly along the axis of the nanobundle in elastomer-based composites, and hence, SWNTs provide load transfer effectiveness. It also implies that SWNTs on the circumference of a nanorope in the composite carry most of the load.

References

1. Saito, R.; Dresselhaus, G.; Dresselhaus, M. S. Physical Properties of Carbon Nanotubes; Imperial College Press: London, 1998.
2. Yu, M. F.; Files, B. S.; Arepalli, S.; Ruoff, R. S. Phys Rev Lett 2000, 84, 5552.
3. Lu, J. P. Phys Rev Lett 1997, 79, 1297.
4. Salvetat, J. P.; Briggs, G. A. D.; Bonard, J. M.; Bacsa, R. R.; Kulik, A. J.; Stockli, T.; Burnham, N. A.; Forro, L. Phys Rev Lett 1999, 82, 944.
5. Hull, D.; Clyne, T. W. An Introduction to Composite Materials; Cambridge University Press: Cambridge, UK, 1996.
6. Wang, M. J. Rubber Chem Technol 1998, 71, 520.
7. George, S. C.; Ninan, K. N.; Groeninickx, G.; Thomas, S. J Appl Polym Sci 2000, 78, 1280.
8. González, L.; Rodriguez, A.; Maras, A. Recent Res Dev Polym Sci 1998, 2, 485.
9. Boonstra, B. B. Polymer 1979, 20, 691.
10. Wolf, S.; Wang, M. J. Rubber Chem Technol 1992, 65, 329.
11. Wolf, S. Rubber Chem Technol 1996, 69, 325.
12. Vu, Y. T.; Mark, J. E.; Pham, L. H.; Engelhardt, M. J Appl Polym Sci 2001, 82, 1391.
13. Donnet, J. B. Rubber Chem Technol 1998, 71, 323.
14. Wolff, S.; Donnet, J. B. Rubber Chem Technol 1990, 63, 32.
15. Guth, E. J Appl Phys 1945, 16, 20.
16. Guth, E.; Simba, R.; Gold, O. Kollid Z 1936, 74, 266.
17. Ding, R.; Leonov, A. I.; Coran, A. Y. Rubber Chem Technol 1996, 69, 81.
18. Rao, A. M.; Jorio, A.; Pimenta, M.; Dantas, M. S.; Saito, R.; Dresselhaus, G.; Dresselhaus, M. S. Phys Rev Lett 2000, 84, 1820.
19. Brown, S. D.L Jorio, A.; Dresselhaus, G.; Dresselhaus, M. S. Phys Rev B 2000, 64, 73403.
20. Hiura, H.; Ebbesen, T. W.; Tanikagi, K.; Takahashi, H. Chem Phys Lett 1993, 202, 509.
21. Iliev, M. N.; Litvinchuk, A. P.; Arepalli, S.; Nikolaev, P.; Scott, C. D. Chem Phys Lett 2000, 316, 217.
22. Rao, A. M.; Richter, E.; Bandow, S.; Chase, B.; Eklund, P. C.; Williams, K. A.; Fang, S.; Subbaswamy, K. R.; Menon, M.; Thess, A.; Smalley, R. E.; Dresselhaus, G.; Dresselhaus, M. S. Science 1997, 275, 187.
23. Rinzler, A. G.; Liu, J.; Dai, H.; Nikolaev, P.; Huffman, C. B.; Rodriguez-Macias, F. J.; Boul, P. J.; Lu, A. H.; Smalley, R. E. Appl Phys A 1998, 67, 29.
24. Hadjiev, V. G.; Iliev, M. N.; Arepalli, S.; Nikolaev, P.; Files, B. S. Appl Phys Lett 2001, 78, 3193.